9-7-2017

# Ambipolar spin diffusion in p-type GaAs: A case where spin diffuses more than charge

F. Cadiz

V. Notot

J. Filipovic

Christopher P. Weber
*Santa Clara University*, cweber@scu.edu

L. Martinelli

***See next page for additional authors***



## Recommended Citation

Cadiz, F., Notot, V., Filipovic, J., Paget, D., Weber, C. P., Martinelli, L., … Arscott, S. (2017). Ambipolar spin diffusion in p-type GaAs: A case where spin diffuses more than charge. Journal of Applied Physics, 122(9), 095703. https://doi.org/10.1063/1.4985831

# Ambipolar spin diffusion in p-type GaAs: A case where spin diffuses more than charge

F. Cadiz,[1,2] V. Notot,[1] J. Filipovic,[1] D. Paget,[1] C. P. Weber,[3] L. Martinelli,[1] A. C. H. Rowe,[1] and S. Arscott[4]

[1]*Physique de la matière condensée, Ecole Polytechnique, CNRS, Université Paris Saclay, 91128 Palaiseau, France*
[2]*Université de Toulouse, INSA-CNRS-UPS, 31077 Toulouse Cedex, France*
[3]*Department of Physics, Santa Clara University, 500 El Camino Real, Santa Clara, California 95053-0315, USA*
[4]*Institut d'Electronique, de Microélectronique et de Nanotechnologie (IEMN), University of Lille, CNRS, Avenue Poincaré, Cité Scientifique, 59652 Villeneuve d'Ascq, France*

(Received 31 May 2017; accepted 27 July 2017; published online 5 September 2017)

We investigate the diffusion of charge and spin at 15 K in p-type GaAs, combining transient-grating and energy-resolved microluminescence measurements to cover a broad range of photoelectron density. At very low optical power, in a unipolar nondegenerate regime, charge and spin diffuse at the same rate, implying that the spin-drag effects are negligible. Upon increasing the photoelectron concentration up to about $10^{16}\,\mathrm{cm}^{-3}$, the charge diffusion constant decreases because of ambipolar electrostatic interactions with the slower-diffusing holes while the spin diffusion constant is reduced only weakly by the ambipolar interaction. A further increase in the excitation power causes increases in both the charge and spin diffusion constants as a consequence of the Pauli principle since the photoelectron gas becomes degenerate. *Published by AIP Publishing.*
[http://dx.doi.org/10.1063/1.4985831]

## I. INTRODUCTION

Numerous investigations of charge and spin transport in semiconductors have led to the conclusion that spin degrees of freedom may be transported independently of charge, due to the effects of spin-orbit interactions,[1–7] of the Pauli principle under degeneracy,[8,9] or of spin Coulomb drag.[10,11] In the latter case, collisions between electrons of opposite spins reduce the spin diffusion constant, making it smaller than the charge diffusion one.

In the present work, we show a unique case where, in p-doped GaAs at 15 K, the effective spin diffusion constant can be larger than the charge one. This is because the electrostatic interaction with holes affects spin diffusion less than charge diffusion. Using a doped p-type GaAs film (Be acceptor concentration $N_A = 1.5 \times 10^{17}\,\mathrm{cm}^{-3}$, thickness $d = 3\,\mu\mathrm{m}$), we measure charge and spin diffusion constants in a wide range of photoelectron concentrations, using a combination of two complementary techniques. Charge and spin transient gratings[12,13] give absolute values of the charge and spin diffusion constants at a relatively high carrier density. CW spatially resolved microphotoluminescence ($\mu$PL)[14,15] gives estimates of charge and spin diffusion constants. Above $10^{16}\,\mathrm{cm}^{-3}$, the charge and spin diffusion constants increase because of the effect of the Pauli principle. Conversely, at a low density, one observes a decrease in the charge diffusion constant caused by ambipolar couplings with holes. In contrast with charge diffusion, and in agreement with theoretical predictions, ambipolar coupling weakly affects spin diffusion so that, in the whole explored range of excitation powers, the spin diffusion constant is larger than the charge diffusion one.

## II. CHARGE AND SPIN TRANSIENT GRATINGS

In a transient-charge-grating experiment, a pair of "pump" laser pulses is simultaneously incident on the sample. The pulses are non-collinear and they interfere. Their absorption excites photocarriers in a sinusoidal pattern of the wavevector $q$. By locally modifying the index of refraction, the photocarriers create a "grating" off of which the probe pulses, arriving later, diffract, and the diffraction is measured as a function of the time delay. The grating's amplitude and the diffracted signal may decay due to two mechanisms: diffusion of charge from the grating's peaks to its troughs, with a charge diffusion constant $D_c^g$, and photocarrier recombination, with the time constant $\tau$. The total decay rate is $1/\tau_c^g = D_c^g q^2 + 1/\tau$, and so measuring the grating's decay at several $q$ determines $D_c^g$.

Conversely, if the two pump beams have crossed linear polarizations,[12] then it is the photoelectrons' *spins* that are modulated sinusoidally, while their density is spatially constant. Thus, the grating is a pure spin grating, and the ambipolar effects are negligible. The grating's amplitude decays at the rate $1/\tau_s^g = D_s^g q^2 + 1/\tau_s$, because of recombination and spin relaxation ($1/\tau_s$) and unipolar spin diffusion ($D_s^g$).

In our experiments, the pulses that form the transient grating had 100 fs duration, and the grating's wavevector $q$ ranged from 1.5 $\mu\mathrm{m}^{-1}$ to 6.29 $\mu\mathrm{m}^{-1}$. The initial photoelectron concentration was varied from $1.4 \times 10^{16}$ $\mathrm{cm}^{-3}$ to $1.6 \times 10^{17}$ $\mathrm{cm}^{-3}$. As described in Ref [16], a probe beam allowed heterodyne detection of the diffracted signal.

The measured decays of charge and spin gratings for selected values of $q$ appear in Fig. 1. For both, the signal $S$ is well described by a fast decay with time $\tau_1$, which weakly depends on $q$ and is related to photoelectron cooling. This

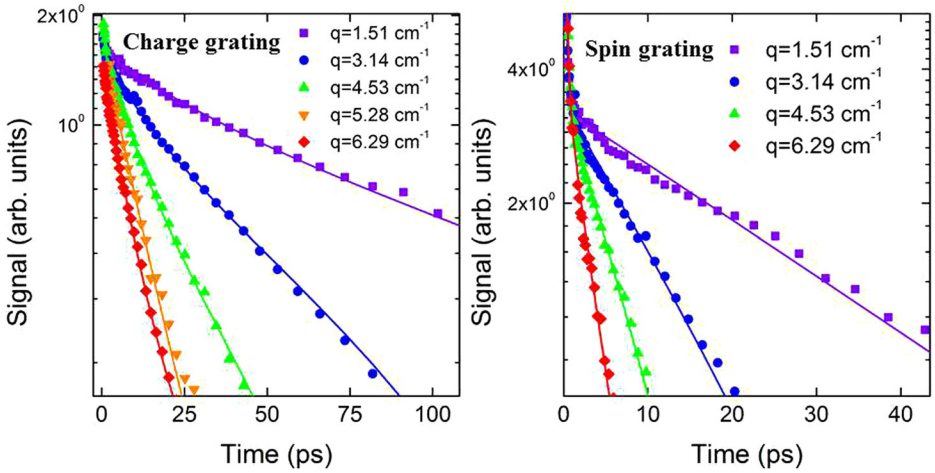


FIG. 1. The left panel shows the signal diffracted from the transient charge grating, for an initial photoelectron concentration of $1.6 \times 10^{17}$ cm$^{-3}$. The right panel shows the signal diffracted from the spin grating at the same laser power. The diffracted signal decays more quickly for gratings of higher wave vector $q$, due to diffusion of photoelectrons and spins; from these decays, the ambipolar charge diffusion and unipolar spin diffusion coefficients may be determined.

signal is followed by a slower, $q$-dependent decay with time $\tau_2$, with a small constant term

$$S(t) = A_1 e^{-t/\tau_1} + A_2 e^{-t/\tau_2} + A_3. \quad (1)$$

For the charge grating, the fast transient is several picoseconds, while the slower transient ranges from 10 ps to 100 ps. Since this time is shorter than the recombination time,[17] the grating's decay owes mainly to charge diffusion. Indeed, the plot of $1/\tau_2$ vs $q^2$ in Fig. 2 shows a pronounced slope due to diffusion, while its intercept $1/\tau$ is too small to determine reliably. Similarly, Fig. 2 shows that the spin grating's decay owes almost entirely to spin diffusion, rather than relaxation.

The diffusion coefficients obtained from the transient grating are summarized in Table I as a function of electron concentration at $t = 0$, which is directly related to the excitation power. Note that both diffusion constants increase with electron concentration and that the spin diffusion constant remains larger than the charge diffusion one.

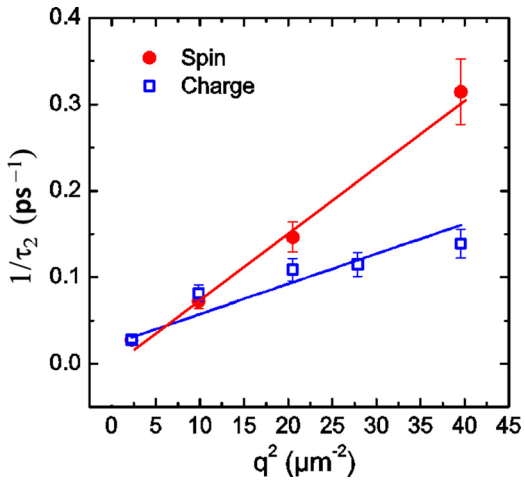


FIG. 2. The squares show the dependence of the inverse decay time $\tau_2$ of the charge grating, defined by Eq. (1), as a function of $q^2$ under the same conditions as Fig. 1. The dependence is approximately linear and the charge ambipolar diffusion constant $D_c^g$ is obtained from the slope of this dependence. The closed circles show the same analysis for the spin grating, which gives the spin diffusion constant $D_s^g$. It is clear from the slopes that the spin diffusion constant is larger than the charge one.

## III. μPL INVESTIGATION OF CHARGE AND SPIN TRANSPORT

### A. Principle

For $\mu$PL investigations, as described in Ref. 14, the sample is excited by a tightly focused, continuous laser beam (Gaussian radius $\sigma \approx 0.6\,\mu$m, energy 1.59 eV). Liquid crystal modulators are used to control the helicity of the excitation and to select the $\sigma^{\pm}$-polarized components of the luminescence, of intensity $I(\sigma^{\pm})$, so that the total luminescence intensity is given by $I = I(\sigma^+) + I(\sigma^-)$. It is also possible to monitor the difference signal, defined as $I_D = I(\sigma^+) - I(\sigma^-)$, and the luminescence degree of circular polarization $\mathscr{P}_L = I_D/I$. The emitted light is focussed on the entrance slit of a spectrometer equipped with a CCD camera as a detector. An image given by this camera is shown in Fig. 3, for an intermediate excitation power of 100 $\mu$W. A cut of the image along the x axis, perpendicular to the entrance slit, gives the local luminescence spectrum at a given distance from the excitation spot.

The normalized local luminescence spectra, obtained from an area of radius 0.4 $\mu$m centered on the excitation spot, are shown in the bottom panel of Fig. 4 for selected excitation powers. The spectra of the luminescence degree of circular polarization are shown in the top panel. This emission has been characterized by an independent study using time-resolved photoluminescence, which has led to the following conclusions.[17] First, at very low power [curves (a) and (b)], the luminescence spectra mostly

TABLE I. Measured values of the effective charge and spin diffusion constants, as found from charge and spin gratings as a function of initial photoelectron concentration. Values inside parentheses are the uncertainties in the measurements.

| Electron concentration ($\times 10^{17}$ cm$^{-3}$) | $D_s^g$ (cm$^2$/s) | $D_c^g$ (cm$^2$/s) |
|---|---|---|
| 0.4 | 45(1) | 21(3) |
| 0.75 | 55(3) | 25(8) |
| 1.6 | 80(7) | 27(6) |
| 2 | 95(3) | 32(2) |
| 3 | 115(10) | 40(5) |

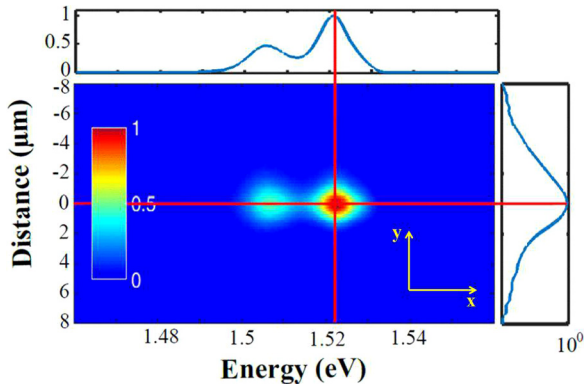


FIG. 3. Image of the intensity collected by the CCD camera at 15 K and for an excitation power of 100 $\mu$W. The spectrometer slit is along the y direction so that the section of the image along the x-axis gives the luminescence spectrum at a given distance from the laser spot (see the top inset for a luminescence spectrum at the laser spot position). This spectrum reveals the BB emission near 1.52 eV and the $eA_0$ one at 1.505 eV. In the same way, a section of the image along the y axis gives the luminescence intensity profile along a line on the sample, at the corresponding energy. For the BB emission, such profile is shown in the right inset.

exhibit the $eA_0$ emission near 1.505 eV, while the weaker emission near 1.52 eV is associated with excitons trapped at neutral acceptors ($A_0X$). The high energy tail, up to 1.53 eV, has been attributed to free excitons formed with heavy and light holes. This excitonic nature of the recombination is responsible for the structure of the polarization spectrum in the 1.52–1.53 eV range, because of unavoidable sample strain at a low temperature which removes the degeneracy between light and heavy hole states. Second,

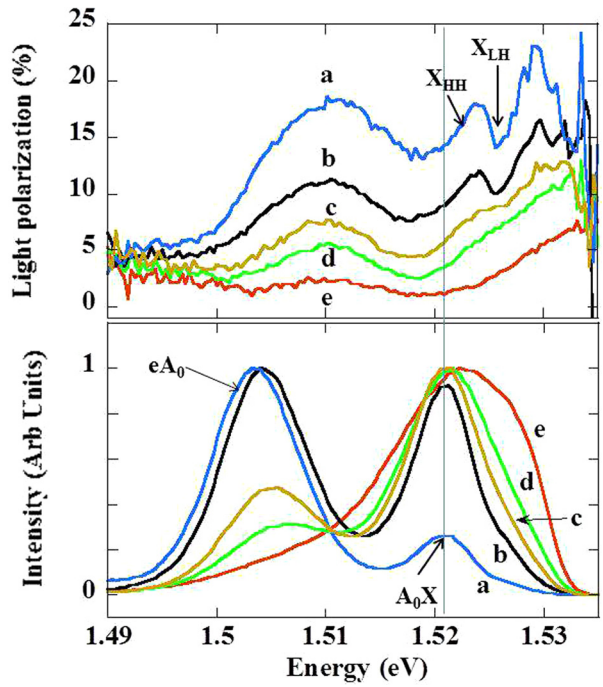


FIG. 4. The bottom panel shows the normalized local luminescence spectra at 15 K for an excitation power equal to 0.21 $\mu$W (a), 24 $\mu$W (b), 0.11 mW (c), 0.35 mW (d), and 2.18 mW (e) and reveals the cross-over between a low power regime where the $eA_0$ recombination is dominant to a high power one, where the BB emission prevails. The top panel shows the spectra of the luminescence degree of circular polarization in the same conditions and reveals a decrease of polarization in the high-power regime.

curves (d) and (e) of the bottom panel of Fig. 4, obtained at high power, correspond to a distinct regime, in which the structure in the polarization spectrum disappears, revealing that the emission peaking at 1.52 eV rather has a band-to-band (BB) nature. In this range, the concentration of photoexcited holes $p$ becomes larger than that of dark holes $p_0$ ($\approx 10^{16}$ cm$^{-3}$ at 50 K), and the exciton formation is prohibited because of screening by holes. This screening occurs as soon as the electron concentration becomes larger than $10^{16}$ cm$^{-3}$.[18] In the same way, at high power, the photoelectron polarization strongly decreases because of exchange interaction with the valence holes.[17]

The excitation-power-induced change of the luminescence spectrum reveals the distinct kinetics of the $eA_0$ line and of the line near 1.52 eV attributed to BB or exciton emission depending on excitation power ($BB/A_0X$). In the case of the acceptor emission, since acceptors remain essentially neutral because of the fast hole trapping,[19] the acceptor recombination time $\tau_A$ is independent of power. The intensity of the $eA_0$ emission is given by

$$I_{eA_0} = \frac{C}{\tau_A}\int_0^d e^{-\alpha(eA_0)z} n(r,z)dz, \tag{2}$$

where $n(r, z)$ is the photoelectron concentration, $r$ is the distance to the excitation spot, and $z$ is the depth. Here, $C$ is a constant, and $\alpha$ is the absorption coefficient at the luminescence energy. This intensity is proportional to the depth-integrated concentration $\langle n(r)\rangle = (1/d)\int_0^d e^{-\alpha(eA_0)z} n(r,z)dz$. On the other hand, for the BB emission, and assuming local charge neutrality,[20] the recombination rate is proportional to $K_{BB}[n(r,z)+p_0]$, where the bimolecular coefficient $K_{BB}$ has been calculated before,[21] so that the BB luminescence intensity becomes dominant at high excitation, at which it increases like $n^2$. It is concluded that the monitoring of the charge spatial diffusion should rather be performed from the spatial profile of the acceptor emission, which gives the spatial profile of the depth average $\langle n(r)\rangle$ of the photoelectron concentration.

A similar analysis shows that the difference signal on the $eA_0$ emission is given by

$$I_{DeA_0} = \frac{C}{2}\left[\frac{1}{\tau_A}+\frac{1}{T_1}\right]\int_0^d e^{-\alpha(eA_0)z} s(r,z)dz, \tag{3}$$

where $s(r, z)$ is the spin density and $T_1$ is the spin relaxation time. Thus, the monitoring of the acceptor difference signal allows us to determine the average over depth of the spin density.

Conversely, a cut of the image along the y axis gives the spatial intensity profile at the corresponding energy, along a line on the sample parallel to the spectrometer entrance slit (the origin of ordinates denoting the distance to the excitation spot). Under focused light excitation, neglecting for simplicity the possible thermoelectric effects, the spatial profiles of the intensity and difference signals are determined by the diffusion equations, which are in steady-state

$$(g_+ + g_-) - n/\tau + \frac{1}{e}\vec{\nabla}\cdot(\vec{J}_e) = 0, \tag{4}$$

$$(g_+ - g_-) - s/\tau_s + \frac{1}{e}\vec{\nabla}\cdot(\vec{J}_s) = 0. \quad (5)$$

Here, $g_\pm$ are the generation rates for $\pm$ spins, $e$ is the absolute value of the electronic charge, $1/\tau = K_{BB}(n+p_0) + 1/\tau_A$ is the total lifetime taking into account acceptor and BB recombination, and $1/\tau_s = 1/\tau + 1/T_1$. The photoelectron diffusion current is given by $\vec{J}_e = eD_c^\mu \vec{\nabla} n$, and the spin diffusion current is given by $\vec{J}_s = eD_s^\mu \vec{\nabla} s$. Here, $D_c^\mu$ and $D_s^\mu$ are the effective local charge and spin diffusion constants which appear in the microluminescence profile. These two quantities take into account ambipolar effects and the Pauli principle[9,13,22] and their expressions will be given in Sec. IV. Note that the Pauli principle also introduces a coupling between these equations. This coupling is weak in the present case and will be neglected.[9,23]

### B. Determination of effective charge and spin diffusion constants

For very low concentrations, the effects of ambipolar diffusion and of the Pauli principle are negligible, and the charge and spin diffusion constants $D_c^\mu$ and $D_s^\mu$ have concentration-independent values denominated by $D_c^0$ and $D_s^0$. They can be evaluated using combined measurements of spatial diffusion profiles and of time-resolved measurements of the relevant lifetimes.[24] The bottom panel of Fig. 5 shows the $eA_0$ intensity spatial profiles for an excitation power of 320 nW, while the top panel shows the corresponding profile of the difference signal. At very low power, the lifetime is mostly determined by recombination at acceptors $\tau_A$. As shown in the figure, the two profiles have a nearly exponential background at a distance larger than about 10 $\mu$m. After subtraction of this background, the spatial profile at a distance larger than 2 $\mu$m, can be approximated by an exponential, from which we find $L = \sqrt{D_c^0\tau_A} = 1.3\pm0.05$ $\mu$m and $L_s = \sqrt{D_s^0\tau_s} = 1.02\pm0.05$ $\mu$m. Using $\tau = 0.9\pm0.05$ ns and $\tau_s = 0.5\pm0.05$ ns,[17] we obtain the charge $D_c^0 = 18.2\pm3$ cm$^2$/s and spin $D_s^0 = 20.8\pm3$ cm$^2$/s diffusion constants at low power.

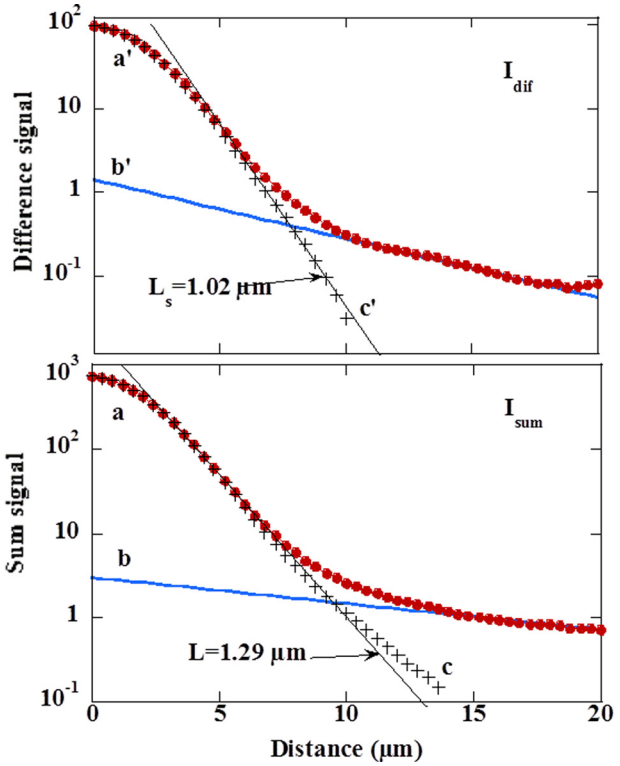


FIG. 5. Curve (a) (bottom panel) shows the sum spatial profile for the $eA_0$ emission at 15 K for an excitation power of 320 nW. Curve (b) shows an exponential fit of the background signal, while curve (c) shows the spatial profile after the removal of the background. This curve gives a charge diffusion length of $L = 1.29$ $\mu$m. The top panel shows the spatial profile of the difference signal in the same conditions and gives a spin diffusion length of $L_s = 1.02$ $\mu$m.

This finding deserves three comments. First, the photoelectron charge and spin diffusion constants $D_c^0$ and $D_s^c$ are equal within the measurement uncertainties. This implies that spin drag[10] is negligible so that the ratio $\tau_m/\tau_{ee}$ of the charge collision time and of the electron-electron spin exchange collision time is small. Indeed, we calculate that, at low excitation power, this ratio is of the order of $10^{-2}$ and decreases with excitation power when the electron and hole concentrations are increased, since holes very efficiently screen the electron-electron exchange interaction.[9] Second, using Einstein's relation, at an electronic temperature of 40 K, we obtain the photoelectron mobility $\mu_e = 5400$ cm$^2$/V s. Although, to our knowledge, no independent measurements of $\mu_e$ have been performed at the same temperature, the latter value corresponds with the value found in Ref. [25] in the 100–200 K range. Finally, as shown in the Appendix using profile analysis at variable emission and excitation energies, the measured photoelectron charge and spin diffusion constants are weakly affected by the formation of excitons which has been found to occur at low power. This is because exciton diffusion lengths are very small so that the exciton formation is equivalent to local trapping.

As the excitation power is increased, the effective charge and spin diffusion constants $D_s^\mu$ and $D_c^\mu$ are evaluated from the difference and sum signals at the excitation spot, respectively. Neglecting diffusion along $z$, we find that the charge and spin diffusion time out of the excitation spot, of the order of $\sigma^2/4D_c^\mu \approx 50$ ps, is more than one order of magnitude faster than recombination and a factor of 4 faster than the smallest experimentally measured spin lifetime at a high power of ≈200 ps.[17] The photoelectron depth-integrated concentration at $r = 0$ is then mostly determined by lateral diffusion and given by $\langle n(r=0)\rangle \approx g\sigma^2/4D_c^\mu$.[26] Since $g$ is proportional to the excitation power $P$, and since $\langle n(r=0)\rangle$ is proportional to the acceptor luminescence intensity at the excitation spot $I_{eA_0}$, the quantity $P/I_{eA_0}$ is proportional to $D_c^\mu$ at $r = 0$. The absolute value of $D_c^\mu$ is then obtained using the value at very low power determined earlier. A similar treatment also gives the effective spin diffusion constant $D_s^\mu$.

The results shown in Table II exhibit two regimes. Up to about 0.1 mW, $D_c^\mu$ decreases by about a factor of 3 to a typical value of 5 cm$^2$/s. For a larger excitation power, one observes an increase of $D_c^\mu$ which overcomes the decrease due to ambipolar effects. A key result of the present work is that throughout the range of excitation power, the spin diffusion constant $D_s^\mu$ is larger than the charge one. The decrease

TABLE II. Measured values of the effective charge and spin diffusion lengths as a function of excitation power. Values inside parentheses give the uncertainties.

| Power | $D_c^\mu$ (cm$^2$/s) | $D_s^\mu$ (cm$^2$/s) |
|---|---|---|
| 320 nW | 18.2 (3) | 20.8 (3) |
| 1.2 $\mu$W | 17.3(3) | 17.6(3) |
| 17.3 $\mu$W | 4.7 (0.5) | 9.1(1) |
| 23.5 $\mu$W | 4.5 (0.5) | 9.0(1) |
| 0.1 mW | 5.4(0.5) | 16.7(3) |
| 0.34 mW | 11.7(1) | 44 (4) |

in $D_s^\mu$ at a relatively weak power is smaller than that of the charge diffusion constant and, at high power, its value is comparable with that measured using spin gratings. The purpose of Sec. IV. is to explain these results.

## IV. INTERPRETATION

### A. Model

Here, we give expressions for the charge and spin diffusion constants obtained using both transient gratings and microluminescence, taking into account ambipolar diffusion and the effect of the Pauli principle.[9,13,22,27] The spin diffusion constant found using transient spin gratings has a relatively simple expression since the photoelectron concentration is spatially homogeneous so that no ambipolar effects are present. One has

$$D_s^g = D_c^0 \nu(n), \tag{6}$$

where the quantity $\nu(n)$ takes into account mostly the effect of the Pauli principle on the spin stiffness, since the possible contribution of the mobility to the concentration dependence of $\nu(n)$ is weak because of screening by holes of electron collisions with ionized impurities. One has

$$\nu(n) = \frac{\mathscr{F}^*_{1/2}[\eta(n)]}{\mathscr{F}^*_{-1/2}[\eta(n)]}, \tag{7}$$

where $\mathscr{F}^*_i$ is the Fermi function of index $i$, and $\eta(n)$ is related to the Fermi energy $E_F$ by $\eta(n) = E_F/k_BT_e$, where $k_B$ is Boltzmann's constant and $T_e$ is the temperature of the photoelectron gas. In order to calculate the ambipolar diffusion constants, it is necessary to couple the diffusion equations [Eqs. (4) and (5)] with the corresponding diffusion equation for holes. As performed elsewhere,[13,22,28] one obtains the internal electric field of ambipolar origin, from which one finds the common value of the charge diffusion constants, given by

$$D_c^\mu = D_c^g = \frac{\sigma_e D_h + \sigma_h D_e}{\sigma_e + \sigma_h}, \tag{8}$$

where $D_h$ is the hole diffusion constant, $D_e = D_c^0\nu(n)$ is the unipolar electron diffusion constant, and the conductivities $\sigma_e = e\mu_e n$ and $\sigma_h = e\mu_h(p + p_0)$ are related to the electron and hole mobilities, $\mu_e$ and $\mu_h$, respectively. Using the Einstein equation for electrons and holes, this equation becomes

$$D_c^\mu = D_c^g = D_c^0 \frac{(p_0 + n)\nu(n) + n}{p_0 + n[1 + \mu_e/\mu_h]}. \tag{9}$$

In this equation, the factor $\nu(n)$, larger than unity, gives the diffusion constant increase caused by the Pauli principle, while the decrease in $D_c^\mu$ caused by ambipolar effects mostly appears in the denominator, and is stronger when the ratio $\mu_e/\mu_h$ of electron and hole mobilities increases.

A similar procedure shows that the spin current is given by $\vec{J}_s = e[D_s\vec{\nabla}s + D'_a\mathscr{P}\vec{\nabla}n]$, where $\mathscr{P} = s/n$ is the spin polarization. The spin diffusion constant obtained by microluminescence is given by

$$D_s^\mu = D_s^g + D'_a\mathscr{P}\frac{\vec{\nabla}n}{\vec{\nabla}s}, \tag{10}$$

where $D_s^g$, given by Eq. (6), is the unipolar spin diffusion constant, and

$$D'_a = D_a^{+-} + D_a^{-+} = \frac{\sigma_e(D_h - D_e)}{\sigma_e + \sigma_h}. \tag{11}$$

This expression can be rewritten

$$D'_a = D_h \frac{1 - \nu(n)\mu_e/\mu_h}{1 + \mu_h(1 + p_0/n)/[\mu_e]}. \tag{12}$$

As seen from Eq. (10), there appears in a spin-spin coupling of ambipolar origin described by a term proportional to $\vec{\nabla}n$.[22] In the limit where the spin polarization $\mathscr{P} = s/n$ is spatially constant, one has $D_s^\mu = D_s^g + D'_a = D_c^\mu$, so that spin diffuses like charge. In the opposite case where spin relaxation is very fast with respect to recombination, near the excitation spot, $s$ strongly decreases with distance, while $\nabla n = 0$. Thus, close to the excitation spot, $D_s^\mu = D_c^0\nu(n)$, so that spin diffusion is unipolar although charge diffusion is ambipolar. This result qualitatively explains why the effective spin diffusion constant is larger than the charge one. In this regime, under the sole effect of ambipolar diffusion (nondegenerate electrons) and assuming $n \gg p_0$ and $\mu_e \gg \mu_h$, the ratio of the charge and spin diffusion lengths is $\sqrt{(D_c^\mu\tau)/(D_s^\mu\tau_s)} \approx \sqrt{(2\mu_h\tau)/(\mu_e\tau_s)}$ and can be smaller than unity for a large ratio $\mu_e/\mu_h$. The physical reason for this effect is that the diffusion of, for instance, spin-up electrons creates an ambipolar electric field that acts on *both* spin species. This coupling induces a decrease in the polarization at the excitation spot, while the spatially averaged polarization is unchanged, thus producing an increase in the spin diffusion constant with respect to the ambipolar charge diffusion constant.[22]

### B. Analysis of the experimental results

In order to compare the results of the two experimental techniques, it is necessary to determine the depth-averaged electronic concentration $\langle n(r=0)\rangle$ in the microluminescence experiments. With this aim, Eqs. (4) and (5) were numerically solved, imposing zero recombination velocity of the front and back surfaces. The values of $D_c^\mu$ and $D_s^\mu$ given

in Table II are shown in Fig. 6 using the calculated values of $\langle n(r=0)\rangle$. While $\mu$PL results concern values of $\langle n(r=0)\rangle$ smaller than $3\times10^{17}$ cm$^{-3}$, transient grating results, also shown in Fig. 6, use larger values.

Immediately apparent is the continuity between the two types of experimental results. For charge transport, the results show that the charge diffusion constant first decreases because of ambipolar diffusion. At a concentration $\langle n(r=0)\rangle \approx 1\times10^{16}$ cm$^{-3}$, which is the onset of degeneracy, the charge diffusion strongly increases due to the effect of the Pauli principle. Recalling that $D_s^g$ is a unipolar spin diffusion constant, the continuity of the spin diffusion constants between the two experimental techniques implies that, at high power, $D_s^\mu$ is little affected by ambipolar diffusion, but essentially depends on the Pauli principle. This is a clear qualitative verification of the above model.

Curve (a) of Fig. 6 shows the unipolar spin diffusion constant $D_s^g$, calculated using Eq. (6) and taking for simplicity a power-independent temperature of the photoelectron gas $T_e = 40$ K, and using the low power values $D_c^0 = D_s^0 \approx 19$ cm$^2$/s. One obtains a very good agreement with the experimental results. In order to verify that this temperature value is reasonable, $T_e$ was estimated from the luminescence spectrum approximately 20 ps after the excitation pulse. For the smallest value of $\langle n(r=0)\rangle$ used for transient gratings ($\langle n(r=0)\rangle = 4\times10^{17}$ cm$^{-3}$), one finds $T_e \approx 45$ K, i.e., a value compatible with the value used for the fit. For the maximum excitation power, one finds $T_e \approx 60$ K, leading to a modification in the theoretical value comparable with the measurement uncertainty.

For comparison of the experimental results obtained by microluminescence with the predictions of Eq. (9), the depth averages of $D_c^\mu$ and $D_s^\mu$ and of $n$, denoted $\langle D_c^\mu\rangle$ and $\langle D_s^\mu\rangle$ and $\langle n\rangle$, respectively, were calculated as a function of depth-averaged concentration. Curve (d) and curve (c) of Fig. 6 give the calculated values of $D_c^\mu$ and $D_s^\mu$, respectively, using $\mu_e/\mu_h = 8$ and are in good agreement with the measurements.

The value of $D_c^g$ at the lowest concentration of $\langle n(r=0)\rangle = 0.4\times10^{17}$ cm$^{-3}$ is also in good agreement with the above calculation [curve (d)]. However, the data points at a higher concentration do not lie on curve (d), but rather on curve (b), obtained using a smaller ratio $\mu_e/\mu_h = 2.5$. The explanation for this finding is at the present time not completely clear. Since the unipolar spin grating data are relatively well interpreted by Eq. (6), we believe that the difference originates from the parameters of ambipolar diffusion. This difference cannot come from the fact that transient gratings involve hotter, nonequilibrium electrons since this would increase the electron mobility, leading to the opposite effect. This effect may be caused by the very strong dependence of the electron mobility ($\approx T_e^{-4.3}$[29]) leading to a significant decrease in $\mu_e$ for relatively weak increases in $T_e$ caused by the increase in light excitation power. Another reason may be the onset of degeneracy of the hole gas, which starts for an electron concentration larger than $\langle n(r=0)\rangle > 10^{17}$ cm$^{-3}$ and may increase the hole mobility.

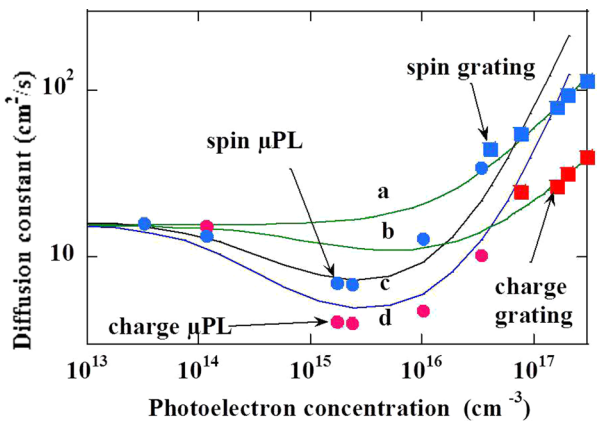


FIG. 6. Summary of the results concerning charge and spin diffusion, as a function of the photoelectron concentration at the excitation spot, with experimental values shown by symbols and calculations by solid lines. The spin diffusivity measured by the transient grating, $D_s^g$, appears as blue squares, while $D_s^\mu$, measured by $\mu$PL, as blue circles. The red squares show the ambipolar charge diffusivity, $D_c^g$, measured by the transient grating, while that measured by $\mu$PL appears as red circles. All calculations use the parameters $D_s^0 = 19$ cm$^2$/s, $D_c^0 = 18$ cm$^2$/s, and an electronic temperature $T_e = 40$ K. The $D_s^g$ data are compared with curve (a), the unipolar spin diffusion calculated from Eq. (6), while $D_s^\mu$ are compared with curve (c), the ambipolar spin diffusion calculated from Eq. (10). The charge diffusion measured by both techniques is ambipolar and calculated from Eq. (9). Curve (d), calculated with $\mu_e/\mu_h = 8$, matches the data well at a low concentration, while curve (b), with $\mu_e/\mu_h = 2.5$, matches the high-concentration data.

## V. CONCLUSION

We have presented a detailed investigation at 15 K of the charge and spin diffusion of a p-type GaAs sample, in the $N_A = 1.5\times10^{17}$ cm$^{-3}$ doping range and of thickness $d = 3$ $\mu$m, as a function of photoelectron concentration. We have used an all-optical approach combining a microluminescence technique (in the $10^{13}$–$10^{16}$ cm$^{-3}$ photoelectron concentration range) with charge and spin transient gratings (for higher photoelectron concentrations, up to several $10^{17}$ cm$^{-3}$). This combination shows that, over a wide range of photoelectron concentrations and as summarized by Fig. 6, the spin diffusion constant remains larger than the charge diffusion one. This difference results from ambipolar effects which slow down charge diffusion up to $n \approx 10^{16}$ cm$^{-3}$ more than spin diffusion. We also observe, for higher concentrations, the strong increase in both diffusion constants because of the Pauli exclusion principle.

The fact that spin diffuses faster than charge because of ambipolar effects is not limited to the sole case of $p^+$ GaAs. More generally, while the ambipolar charge diffusion constant is given by Eq. (11), the second term of Eq. (10) is of the order of $D_a'(2\mathscr{P})^2$, where $D_a'$ is given by Eq. (11).[30] As a result, it is anticipated that reducing the acceptor concentration in the p-type material will increase the magnitude of ambipolar effects and will reduce the photoelectron polarization, thus reducing the ambipolar charge diffusion constant and increasing that of the spin diffusion constant. Similar effects are also expected for the n-type material. In this case, assuming $\sigma_e \gg \sigma_h$, one has $D_a' \approx -D_e$, so that the spin diffusion constant can be arbitrarily close to its unipolar value depending on the value of $\mathscr{P}$ which depends on the relative value of dark and photoelectron concentrations.

## ACKNOWLEDGMENTS

C.P.W. was supported by the National Science Foundation Grant No. DMR-1105553. This work was partly supported by the French RENATECH network.

## APPENDIX A: NEGLIGIBILITY OF EXCITONIC EFFECTS

Here, we show that excitons do not strongly affect the measurement of the charge and spin diffusion constants of the conduction electrons. For this investigation, we analyze the images obtained for a weak excitation power of 201 $\mu$W, and a very low lattice temperature of 6 K, in order to increase the magnitude of possible excitonic effects.

We have compared the diffusion profiles for electron-related energies situated between 1.495 and 1.51 eV in the spectrum and exciton-related emissions lying between 1.515 and 1.53 eV. Curve (a) of Fig. 7 shows the charge diffusion profiles at 1.497 eV corresponding to the $eA_0$ emission. The analysis of curve (a) is performed by removing the background lying at a distance larger than 10 $\mu$m.[31] As shown in curve (c), this correction leaves a decay which corresponds with a single exponential over 3 orders of magnitude, of characteristic length $L = 1.79 \pm 0.1$ $\mu$m. Curve (b) of Fig. 7 shows the charge diffusion profile at an energy of 1.519 eV. With respect to curve (a), one observes a slight additional signal near the excitation spot. However, within experimental accuracy, the excitonic emission is characterized by the same decay length. Qualitatively, this suggests the quasi-absence of exciton diffusion, so that the excitonic profile is determined by the conduction electron one. If one approximates the ratio $L_x/L$, by $(m_e\tau_x)/(m_{hh}\tau_A) \approx 0.09$, where $m_e$ is the conduction electron mass, $m_{hh}$ is the heavy hole mass, and $\tau_x$ is the exciton recombination lifetime, one finds indeed that the exciton diffusion length is of the order of 0.15 $\mu$m.

In order to evaluate the possible modification of the electron diffusion length due to excitons, we have changed the excitation energy. It is anticipated that the exciton concentration will be significantly weaker for an excitation resonant with the $eA_0$ emission, which does not create valence holes. Conversely, resonant excitation at the energy of excitonic emission will increase the relative creation of excitons with respect to conduction electrons. Shown in Fig. 8 is the dependence of the charge diffusion length measured on the $eA_0$ emission as a function of excitation energy. Also shown for reference is the luminescence spectrum. It is seen that the diffusion length weakly depends on excitation energy. No decrease can be seen when the excitation is resonant with the exciton luminescence. A slight increase is observed below 1.51 eV, that is, for dominant excitation from the acceptor levels. This increase may be caused by the increase in the substrate luminescence caused by the weak absorption of the excitation light by the thin sample in this energy range.

In order to interpret in more detail the above results, one uses the photoelectron and exciton rate equations which are, in steady-state, at low excitation power, and neglecting for simplicity the exciton trapping at neutral acceptors

$$0 = g + e_x n_x - (K_x p_0 + 1/\tau_A)n + D_c^0 \Delta n, \tag{A1}$$

$$0 = g_x - (1/\tau_x + e_x)n_x + K_x p_0 n + D_x \Delta n_x, \tag{A2}$$

where $g$ and $g_x$ are the creation rates of electrons and excitons by light excitation, $\tau_A$ and $\tau_X$ are the recombination times for electrons at acceptors and for excitons, and $e_x$ is the exciton rate of dissociation, as evidenced from the presence of a peak in the photoconductivity spectra when the excitation is resonant with the exciton energy.[32] Here, $D_x$ is the exciton diffusion constant. The quantity $K_x$ is the bimolecular exciton formation constant and $p_0$ is the concentration in the valence band. Defining $L = \sqrt{D_c\tau_A/(K_x p_0 \tau_A + 1)}$, $L_x = \sqrt{D_x\tau_x/(e_x\tau_x + 1)}$, one finds that eigenmodes $N_\pm$ given by

$$N_\pm = \left(k_\pm \frac{e_x}{1/\tau_A + K_x p_0} - 1\right) n_x + \left(\frac{K_x p_0}{1/\tau_x + e_x} - k_\pm\right) n \tag{A3}$$

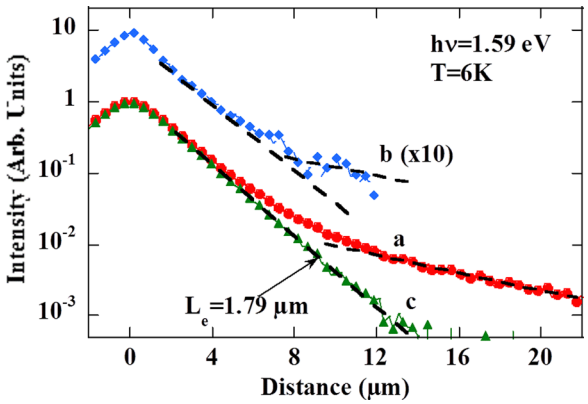


FIG. 7. Curve (a) shows the charge diffusion profile at an emission energy of 1.497 eV corresponding to the $eA_0$ emission and reveals the spatial diffusion of photoelectrons. Curve (b) shows the charge diffusion profile at an emission energy of 1.519 eV and reveals the effective spatial diffusion of excitons. Curve (c) is obtained from curve (a) by removing the tail at a large distance caused by the luminescence of the substrate, and closely corresponds with curve (b), implying that the spatial diffusion profiles of electrons and excitons are characterized by the same lengths.

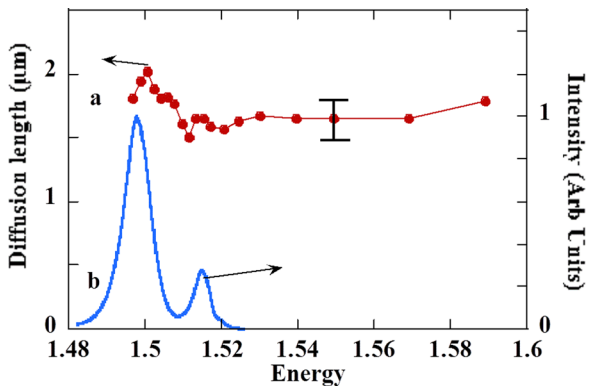


FIG. 8. Curve (a) shows the dependence of the photoelectron diffusion length, measured as shown by curve (c) of Fig. 7 at the acceptor luminescence energy, as a function of excitation energy. Curve (b) shows for comparison the luminescence spectrum for excitation at 1.59 eV. Apart from a slight increase near 1.50 eV, the diffusion length does not depend on excitation energy, although the ratio of the electron and exciton concentrations is strongly modified.

have a diffusion length given by

$$\mathscr{L}_{\pm}^2 = \frac{2L_x^2L^2}{\left(L^2+L_x^2\right)\pm\mathscr{A}}. \tag{A4}$$

Here

$$k_{\pm} = \frac{1}{2L^2}\left[\frac{K_x p_0 \tau_A + 1}{e_x \tau_A}\right]\left[\left(L^2 - L_x^2\right)\pm\mathscr{A}\right], \tag{A5}$$

where $\mathscr{A} = \sqrt{\left(L^2 - L_x^2\right)^2 + 4\beta L^2 L_x^2}$ and $\beta$, given by

$$\beta = \frac{K_x p_0 \tau_A}{K_x p_0 \tau_A + 1}\frac{e_x \tau_x}{e_x \tau_x + 1} \tag{A6}$$

is a measure of the electron/exciton coupling caused by exciton formation and dissociation. The photoelectron and exciton concentrations are given by

$$2n(1-\beta) = \frac{e_x\tau_A}{K_x p_0 \tau_A + 1}\left[(N_+ - N_-)\frac{\left(L_x^2+L^2\right)}{\mathscr{A}} + (N_+ + N_-)\right], \tag{A7}$$

$$2n_x(1-\beta) = (N_+ - N_-)\frac{\left[L_x^2 + L^2(2\beta - 1)\right]}{\mathscr{A}} + (N_+ + N_-), \tag{A8}$$

and exhibit two successive decay lengths, $\mathscr{L}_{\pm}^2$, for which the relative amplitudes can be obtained from Eqs. (A7) and (A8). The fact that, as shown in curve (c) of Fig. 7, only one exponential decay length is observed implies that the spatial transient corresponding with $\mathscr{L}_+$ cannot be resolved. Using Eq. (A4), and the above value of $L_x/L$, one estimates $\mathscr{L}_+/\mathscr{L}_- < 0.1$ implying that $\mathscr{L}_+ \approx 0.2\,\mu$ m. This is indeed smaller than the Gaussian radius of the laser spot, of 0.6 $\mu$m. The experimental results can then be understood by neglecting the exciton diffusion term in Eq. (A2), in which case one has $n_x(1/\tau_x + e_x) = K_x p_0 n + g_x$. This equation implies that, as observed in Fig. 7, the exciton luminescence profile is identical to the electron one except near the excitation spot, where $g_x$ can be significant. This slightly larger exciton luminescence near the excitation spot is observed experimentally in Fig. 7. Using this expression of $n_x$ in Eq. (A3), we finally obtain the uncoupled diffusion equation for electrons

$$0 = g + g_x\frac{e_x\tau_x}{e_x\tau_x+1} - (K_x p_0 + 1/\tau_A)(1-\beta)n + D_c^0\Delta n. \tag{A9}$$

This equation shows that exciton formation and dissociation results in an increase of the effective lifetime by $1-\beta$ and of the diffusion length by $\sqrt{1-\beta}$, but that the diffusion constant is unaffected by excitonic effects.


[1] A. Balocchi, Q. H. Duong, P. Renucci, B. L. Liu, C. Fontaine, T. Amand, D. Lagarde, and X. Marie, Phys. Rev. Lett. **107**, 136604 (2011).
[2] S. D. Ganichev, H. Ketterl, W. Prettl, E. L. Ivchenko, and L. E. Vorobjev, Appl. Phys. Lett. **77**, 3146 (2000).
[3] E. M. Hankiewicz and G. Vignale, J. Phys.: Condens. Matter **21**, 253202 (2009).
[4] T. Jungwirth, J. Wunderlich, and K. Olejnik, Nature Mater. **11**, 382 (2012).
[5] J. M. Kikkawa and D. D. Awschalom, Nature **397**, 139 (1999).
[6] Y. K. Kato, R. C. Myers, A. C. Gossard, and D. D. Awschalom, Science **306**, 1910 (2004).
[7] J. D. Koralek, C. P. Weber, J. Orenstein, B. A. Bernevig, S. C. Zhang, S. Mack, and D. D. Awschalom, Nature **458**, 610 (2009).
[8] F. Cadiz, D. Paget, and A. C. H. Rowe, Phys. Rev. Lett. **111**, 246601 (2013).
[9] F. Cadiz, D. Paget, A. C. H. Rowe, T. Amand, P. Barate, and S. Arscott, Phys. Rev. B **91**, 165203 (2015).
[10] I. D'Amico and G. Vignale, Phys. Rev. B **65**, 085109 (2002).
[11] C. P. Weber, N. Gedik, J. E. Moore, J. Orenstein, J. Stephens, and D. D. Awschalom, Nature **437**, 1330 (2005).
[12] A. R. Cameron, P. Riblet, and A. Miller, Phys. Rev. Lett. **76**, 4793 (1996).
[13] C. P. Weber and E. A. Kittlhaus, J. Appl. Phys. **113**, 053711 (2013).
[14] I. Favorskiy, D. Vu, E. Peytavit, S. Arscott, D. Paget, and A. C. H. Rowe, Rev. Sci. Instrum. **81**, 103902 (2010).
[15] D. J. Wolford, G. D. Gilliland, T. F. Kuech, J. A. Bradley, and H. P. Hjalmarson, Phys. Rev. B **47**, 15601 (1993).
[16] A. A. Maznev, K. A. Nelson, and J. A. Rogers, Opt. Lett. **23**, 1319 (1998).
[17] D. Lagarde, P. Renucci, F. Cadiz, D. Paget, T. Amand, A. C. H. Rowe, and S. Arscott, Appl. Phys. Lett. **110**, 082101 (2017).
[18] G. W. Fehrenbach, W. Schafer, J. Treusch, and R. G. Ulbrich, Phys. Rev. Lett. **49**, 1281 (1982).
[19] D. Bimberg, H. Munzel, A. Steckenborn, and J. Christen, Phys. Rev. B **31**, 7788 (1985).
[20] F. Cadiz, D. Paget, A. C. H. Rowe, L. Martinelli, and S. Arscott, Appl. Phys. Lett. **107**, 162101 (2015).
[21] W. P. Dumke, Phys. Rev. **105**, 139 (1957).
[22] F. Cadiz, D. Paget, A. C. H. Rowe, and S. Arscott, Phys. Rev. B **92**, 121203(R) (2015).
[23] It has been shown in Ref. 9 that, at high excitation the Pauli Principle introduces a spin charge coupling which modifies both the concentration and the spin polarization. These effects are of first order in the spin polarization for the spin density and of second order for the concentration. In the present case, under degenerate conditions, the polarization is rather weak, so that the effects of this coupling will be neglected.
[24] F. Cadiz, P. Barate, D. Paget, D. Grebenkov, J. P. Korb, A. C. H. Rowe, T. Amand, S. Arscott, and E. Peytavit, J. Appl. Phys. **116**, 023711 (2014).
[25] H. Ito and T. Ishibashi, J. Appl. Phys. **65**, 5197 (1989).
[26] D. Paget, F. Cadiz, A. C. H. Rowe, F. Moreau, S. Arscott, and E. Peytavit, J. Appl. Phys. **111**, 123720 (2012).
[27] M. E. Flatté and J. L. Byers, Phys. Rev. Lett. **84**, 4220 (2000).
[28] H. Zhao, M. Mower, and G. Vignale, Phys Rev. B **79**, 115321 (2009).
[29] F. Cadiz, D. Paget, A. C. H. Rowe, E. Peytavit, and S. Arscott, Appl. Phys. Lett. **106**(9), 092108 (2015).
[30] Approximating $\vec{\nabla} n$ by $n/L$ and $\vec{\nabla} s$ by $s/L_s$, one finds that the second term of Eq. (10) is of the order of $D_a' L_s/L \approx D_a'(2\mathscr{P})^2$.
[31] The reasons for this background are not completely clear at the present time. The background cannot be due to luminescence of the semi-insulating substrate, since it is still present if one removes the substrate. We believe it may originate from photon recycling in the sample plane. Further experiments are necessary in order to clarify its origin.
[32] C. Richard and M. Dugue, Phys. Stat. Sol. (b) **50**, 263 (1972).